RESEARCH PAPER

Hypoxia augments the calcium-activated chloride current carried by anoctamin-1 in cardiac vascular endothelial cells of neonatal mice

Ming-Ming Wu[1], Jie Lou[1], Bin-Lin Song[1], Yuan-Feng Gong[1], Yan-Chao Li[1], Chang-Jiang Yu[1], Qiu-Shi Wang[1], Tian-Xing Ma[1], Ke Ma[1], H Criss Hartzell[2], Dayue Darrel Duan[3], Dan Zhao[1] and Zhi-Ren Zhang[1]

[1]*Departments of Clinical Pharmacy and Cardiology, Institute of Clinical Pharmacy, The 2nd Affiliated Hospital, Key Laboratories of Education Ministry for Myocardial Ischemia Mechanism and Treatment, Harbin Medical University, Harbin, China,* [2]*Department of Cell Biology, Emory University School of Medicine, Atlanta, GA, USA, and* [3]*Laboratory of Cardiovascular Phenomics, Department of Pharmacology, Center for Molecular Medicine, University of Nevada, School of Medicine, Reno, NV, USA*

BACKGROUND AND PURPOSE

The molecular identity of calcium-activated chloride channels (CaCCs) in vascular endothelial cells remains unknown. This study sought to identify whether anoctamin-1 (Ano1, also known as TMEM16A) functions as a CaCC and whether hypoxia alters the biophysical properties of Ano1 in mouse cardiac vascular endothelial cells (CVECs).

EXPERIMENTAL APPROACH

Western blot, quantitative real-time PCR, confocal imaging analysis and patch-clamp analysis combined with pharmacological approaches were used to determine whether Ano1 was expressed and functioned as CaCC in CVECs.

KEY RESULTS

Ano1 was expressed in CVECs. The biophysical properties of the current generated in the CVECs, including the Ca^{2+} and voltage dependence, outward rectification, anion selectivity and the pharmacological profile, are similar to those described for CaCCs. The density of $I_{Cl(Ca)}$ detected in CVECs was significantly inhibited by T16A$_{inh}$-A01, an Ano1 inhibitor, and a pore-targeting, specific anti-Ano1 antibody, and was markedly decreased in Ano1 gene knockdown CVECs. The density of $I_{Cl(Ca)}$ was significantly potentiated in CVECs exposed to hypoxia, and this hypoxia-induced increase in the density of $I_{Cl(Ca)}$ was inhibited by T16A$_{inh}$-A01 or anti-Ano1 antibody. Hypoxia also increased the current density of $I_{Cl(Ca)}$ in Ano1 gene knockdown CVECs.

CONCLUSIONS AND IMPLICATIONS

Ano1 formed CaCC in CVECs of neonatal mice. Hypoxia enhances Ano1-mediated $I_{Cl(Ca)}$ density via increasing its expression, altering the ratio of its splicing variants, sensitivity to membrane voltage and to Ca^{2+}. Ano1 may play a role in the

pathophysiological processes during ischaemia in heart, and therefore, Ano1 might be a potential therapeutic target to prevent ischaemic damage.

Abbreviations
Ano1, anoctamin-1; CaCC, calcium-activated chloride channel; $I_{Cl(Ca)}$, calcium-activated chloride current; CVEC, cardiac vascular endothelial cell

Introduction

Calcium-activated chloride channels (CaCCs) play an important role in epithelial secretion of electrolytes and water, sensory transduction, regulation of neuronal and cardiac excitability, and regulation of vascular tone (Hartzell *et al.*, 2005; channel nomenclature follows Alexander *et al.*, 2013). A member of a Ca^{2+}-sensitive Cl^- channel family (CLCA1), volume-regulated chloride channel (CLC-3), bestrophins and tweety were proposed as the CaCC candidate proteins; however, the biophysical features of the currents mediated by these channels are different from those of native classical CaCCs (Hartzell *et al.*, 2009). Heterologous expression of the proteins anoctamin-1 (Ano1; TMEM16A) and Ano2 (TMEM16B) in a variety of cell types produced calcium-activated chloride currents [$I_{Cl(Ca)}$], with biophysical characteristics similar to those of native classical CaCCs. Therefore, Ano1 and Ano2 have been proposed as the novel candidate proteins for CaCCs (Caputo *et al.*, 2008; Schroeder *et al.*, 2008; Yang *et al.*, 2008; Pifferi *et al.*, 2009). Subsequent studies suggested that the gene product of *Ano1* was the protein involved in native CaCC in gland acinar cells (Yang *et al.*, 2008; Huang *et al.*, 2009; Romanenko *et al.*, 2010), epithelial cells (Ousingsawat *et al.*, 2009; Rock *et al.*, 2009; Dutta *et al.*, 2011), interstitial cells of Cajal (Hwang *et al.*, 2009) and smooth muscle cells (SMCs) (Davis *et al.*, 2010; Manoury *et al.*, 2010).

CaCCs are expressed in various endothelial cell types of different species, including calf pulmonary artery endothelial cells (Nilius *et al.*, 1997), mouse aorta endothelial cells (Suh *et al.*, 1999) and human umbilical vein endothelial cells (Zhong *et al.*, 2000). CaCCs have been implicated in the control of the membrane potential, which helps to maintain the driving force for Ca^{2+}. In vascular endothelial cells, the resting membrane potential (approximately −40 mV) is more negative than the equilibrium potential for Cl^- (approximately −28 mV) (Ono *et al.*, 1998). As a consequence of agonist-induced increase in cytosolic Ca^{2+} ($[Ca^{2+}]_i$), CaCCs are activated and Cl^- leaves the cell, which results in a shift of the membrane potential of endothelial cells towards the Cl^- equilibrium potential, and possibly inducing a negative feedback during agonist stimulation. Therefore, CaCCs are functionally important in the control of the membrane potential, the driving force for Ca^{2+} influx and regulation of Ca^{2+} signalling in endothelial cells (Hosoki and Iijima, 1994). CaCCs may also be involved in control of volume, cell shape and cell proliferation, as well as intracellular pH regulation (Nilius *et al.*, 1997; Hartzell *et al.*, 2005). The CaCCs are involved in many important physiological processes in vascular endothelial cells but their molecular identity and roles in ischaemic conditions remain unknown.

In the present study, we investigated whether Ano1 functions as a CaCC and whether hypoxia alters the biophysical properties of Ano1 in cardiac vascular endothelial cells (CVECs) isolated from neonatal mice. The novel findings of the functional properties of Ano1 in the normal and ischaemic CVECs may provide new therapeutic target for the treatment of ischaemia-induced damage in the vascular system.

Methods

Isolation and culture of CVECs and Ano1 gene silencing in CVECs

All animal care and experimental procedures were approved by the Harbin Medical University Animal Supervision Committee. All studies involving animals are reported in accordance with the ARRIVE guidelines for reporting experiments involving animals (Kilkenny *et al.*, 2010; McGrath *et al.*, 2010). Over 200 animals were used in the experiments described here.

Neonatal BALB/c mice were purchased from Experimental Animal Center of Harbin Medical University. CVECs were isolated from the left ventricles of hearts from neonatal mice, as previously described (Zhou *et al.*, 2010), with slight modifications. Briefly, each pup was placed on a 37°C temperature-controlled pad for general anesthesia from spontaneous respirations of 3.0% isoflurane in oxygen. After anaesthesia, the hearts were quickly excised and washed, then minced in ice-cold serum-free DMEM. The atrial, cardiac valves and right ventricle were stripped under a microscope. Then the isolated left ventricles were immersed in 70% ethanol for 10 s to devitalize epicardial mesothelial and endocardial endothelial cells. The left ventricular tissue was finely minced and transferred into a tube containing 5 mL of trypsin (0.25%) for twice for 5 min at 37°C, in a shaking water bath. Dissociated cells were filtered through a 100 μm mesh filter and centrifuged at 100× *g* for 5 min in a sealed centrifuge (C3i centrifuge, Jouan Laboratories, Saint-Herblain, France). Cells were resuspended in DMEM supplemented with 10% FBS, 100 IU mL^{-1} penicillin and 100 μg mL^{-1} streptomycin, and then transferred into a cell culture dish for 30 min at 37°C in 5% CO_2 incubator to remove the attached fibroblasts. After these procedures, the CVECs were harvested (Zhou *et al.*, 2010) and were identified using CD31 antibody. The non-attached viable CVECs were collected and seeded onto coverslips or dishes for the following experiments. The CVECs reached ~80% confluence within 3–4 days and displayed uniform 'cobblestone' morphology under optical microscope and were ready for the experiments.

Ano1 gene silencing was carried out as follows. CEVCs were cultured in 6-well plates. After cells became 80% confluent, Ano1-specific small hairpin RNAs (shRNAs) were

transfected using lipofectamine 2000 (Invitrogen, Carlsbad, CA, USA). The sequences of shRNA constructs are listed in Supplement Table 1. The shRNAs were cloned into the pGPU6/GFP/Neo-shRNA vector by inserting constructs into the 3′-UTR of the GFP gene (GenePharma, Shanghai, China). Evaluation of gene silencing efficiency assays (qRT-PCR and western blot assays) were performed 48 hrs after transfection. In addition, the green fluorescent protein (GFP) was used as an additional indicator for success of transfection.

Quantitative real-time PCR (qRT-PCR)

Total RNA was extracted from CVECs using TRIzol reagent (Invitrogen, Carlsbad, CA, USA). Reverse transcription was performed with the RT system protocol in a 20 µL reaction mixture. Total RNA (1 µg) was used in the reaction, and a random primer was used for the initiation of cDNA synthesis, the reaction mixture was incubated at 25°C for 10 min, 37°C for 120 min and 85°C for 5 min, respectively. Then qRT-PCR was performed using the ABI Prism 7500 sequence detection system with SYBR Green PCR reagents (Applied Biosystems, USA). The primers used are listed in Supplement Table 1. After circle reaction, the threshold cycle (Ct) was determined and relative Ano1 and Ano2 mRNA levels were calculated based on the Ct values and normalized by β-actin level in each sample.

For determining whether hypoxia leads to an altered expression ratio of Ano1 splicing variants in CVECs, we used the primers listed in Supplement Table 2, in which exons 6b, 13 and 15 were excluded. The values for the mRNA products of these Ano1 splicing variants, obtained either from normoxic or hypoxic condition, were then normalized to the values of Ano1 mRNA product obtained using the primers shown in Supplement Table 3 under normoxic condition.

Western blotting

CVECs were homogenized in RIPA lysis buffer containing 10 µL mL⁻¹ protease inhibitor cocktail, and centrifuged at 13,500g for 15 min at 4°C to precipitate cell debris. Equal concentration of denatured proteins were separated on 10% SDS-polyacrylamide gels and were transferred onto polyvinylidene difluoride (PVDF) membranes, blocked by 5% nonfat dry milk for 1 hr, followed by incubating with rabbit polyclonal anti-Ano1 antibody (Abcam ab53213, 1:500 dilution) for overnight. After washing with TBS-T, the membranes were incubated with horseradish peroxidase-conjugated goat anti-rabbit IgG secondary antibody (Santa Cruz-2793, CA, 1:4000 dilution) for 1 hr, labeled proteins were visualized with enhanced chemiluminescence (ECL) (Invitrogen WP20005, Carlsbad, CA, USA) and quantified by scanning densitometry (Bio-Rad). The intensities of interesting band were normalized by the intensity of β-actin (Santa Cruzsc-47778, 1:1000 dilution) bands.

Immunostaining

Neonatal mouse heart was fixed with 4% paraformaldehyde for 2 hrs followed by 18% sucrose 16 hrs, then preserved in optimum cutting temperature compound (–80°C). Longitudinal sections of the left ventricular wall were cut with a cryostat microtome (CM 3500 cryostat, Israel) at a thickness of 4 mm and permeabilized with 0.2% Triton X-100 (PBST) for 10 min and blocked with 5% bovine serum albumin (BSA) PBST for 1 hr. Rabbit polyclonal anti-Ano1 antibody (1:1000 dilution) (Yu et al., 2010) and sheep polyclonal antibody to von Willebrand factor (vWF) were added in 1% BSA/PBST for overnight at 4°C. The sections were washed in PBST and incubated with Alexa Fluor 488 conjugated donkey anti-rabbit IgG (Invitrogen A21206, 1:1000 dilution) or TRITC conjugated donkey anti-sheep (Abcam ab6897, 1:1000 dilution) for 1 hr.

The endothelial cells of passage one were washed with ice-cold PBS. After fixation with 4% paraformaldehyde at room temperature (22–24°C), cells were permeabilized with 0.2% Triton X-100 in PBS for 10 min and blocked with 5% BSA/PBST for 30 min. Rabbit polyclonal anti-Ano1 antibody (1:1000 dilution) (Yu et al., 2010), endothelial cells markers CD31 (Abcam ab7388, 1:1000 dilution) was added in 1% BSA/PBS overnight at 4°C. Subsequently, the cells were washed in PBS containing 0.1% Tween and incubated with Alexa Fluor 488 conjugated donkey anti-rabbit IgG (Invitrogen A21206, 1:1000 dilution) or Alexa Fluor 594 conjugated donkey anti-rat IgG (Invitrogen A21209, 1:1000 dilution) for 1 hr. All slides were imaged using a confocal microscope (Olympus, Fluoview1000, Japan). Identical acquisition settings were used for all images.

Cell proliferation assays

3-(4, 5-Dimethyl-thiazol-2-yl)-2, 5-diphenyltetrazolium bromide (MTT) assay was employed to evaluate cell proliferation rate. The CVECs were plated into 96-well plates at a density of 50,000 cells per well in 200 µl culture medium. After 8 hrs recovery, cells were treated with 30 µM T16A$_{inh}$-A01 for 48 hrs. For hypoxic group CVECs were cultured under normal condition for 32 hrs and followed by culturing in the hypoxic incubator for 16 hrs, in the absence or in the presence of 30 µM T16A$_{inh}$-A01. Then 20 µl PBS-buffered MTT (5 mg mL⁻¹) solution was added to each well and the cells were incubated at 37°C for 4 hrs. Subsequently, the supernatant was then discarded form each well and 100 µL DMSO was added into each well and mixed thoroughly for 10 min to ensure all crystals were dissolved. The absorbance of samples was measured by a microplate reader at wavelength of 570 nm (Tecan, Mannedorf, Switzerland). The quantity of formazan product would be proportional to the number of living cells in culture.

Exposure of CVECs to hypoxia

For hypoxic treatment, ~80% confluent CVECs were placed in a hypoxic incubator (Thermo Scientific Series WJ 8000, Waltham, MA, USA) and were kept at 37°C for 16 h with a constant stream of water-saturated 93% N_2, 5% CO_2 and 2% O_2. There was no apoptosis that occurred under this condition, as detected by TUNEL assays (data not shown).

Patch-clamp recording

The whole-cell patch-clamp technique was used to record $I_{Cl(Ca)}$ in voltage-clamp mode using an Axopatch 200B amplifier, and data were filtered at 1 kHz and sampled at 5 kHz (Axon Instruments, Foster City, CA, USA). Borosilicate glass electrodes were pulled with a four-stage puller (Sutter, Novato, CA, USA) and had a resistance of 1–2 MΩ when filled

with pipette solution. $I_{Cl(Ca)}$ was recorded using a holding potential of 0 mV followed by voltage steps from –100 to +100 mV in 20 mV increment for a duration of 1000 ms, and then repolarized to –100 mV for 300 ms. Membrane current densities were obtained by dividing the measured current amplitude by the cell capacitance. The current density–voltage relationships (I–V) were plotted using the calculated current density from the beginning (instantaneous) or the end (steady state) of 1000 ms, as a function of voltages. The activation time constant (τ_{act}) and the inactivation time constant (τ_{inact}) were, respectively, obtained by fitting 400 ms of whole-cell current following the end of the capacitance transient and by fitting 200 ms of whole-cell current following the repolarization currents measured after capacitance transient to a single exponential function. The macroscopic chord conductance (G) was calculated by an equation: $G = I/(V_M - V_{rev})$, where I represents the amplitude of steady-state current measured at the end of 1000 ms of each voltage, V_M indicates the membrane potential and V_{rev} is the reversal potential (since V_{rev} is ~0 mV for all records, we set V_{rev} to 0 mV for all calculations). The G obtained from each tested voltage was then normalized to the G calculated from +100 mV (G_{max}, the maximal cord conductance). These data points were plotted as a function of voltages and were fitted by the Boltzmann function: $G = G_{max}/\{1 + exp[-(V_M - V_{1/2})/k]\}$, where $V_{1/2}$ represents the voltage at which 50% of activation occurs and k is the slope factor. Prior to analysis, the whole-cell recording traces were further filtered to 100 Hz (Clampfit 10.2; Molecular Devices, Sunnyvale, CA, USA).

For anion selectivity experiments, the data were corrected for junction potentials at the ground bridge (3 M KCl in 3% agar), which ranged from 2 to 4 mV as determined with a free-flowing KCl electrode. V_{rev} for chloride and for each test anion were used to calculate relative permeability [anion X^- to Cl^- permeability (P_x^-/P_{Cl}^-)] values according to the Goldman–Hodgkin–Katz equation (Hille, 1992).

The extracellular solution contained (in mM): 150 NaCl, 1 $CaCl_2$, 1 $MgCl_2$, 10 glucose, 10 sucrose, 10 HEPES (pH = 7.4 with NaOH); the pipette solution contained (in mM): 130 CsCl, 10 EGTA, 1 $MgCl_2$, 10 HEPES, 1 ATP and different concentrations of $CaCl_2$ to obtain the desired free Ca^{2+} concentration (calculated according to the method posted at http://www.stanford.edu/~cpatton/; 1 mM for 18 nM, 6 mM for 290 nM, 7 mM for 453 nM, 8 mM for 777 nM, 8.5 mM for 1.1 μM, and 10 mM for 36.5 μM) (pH = 7.3 with CsOH), as determined with the Ca-EGTA calculator.

Data analyses

Data are reported as mean values ± SEM for n observations. All data gathered in Excel were plotted using Origin 8.5 software (OriginLab, Northampton, MA, USA). Significance was determined using Student's t-tests for paired or unpaired data. $P < 0.05$ was considered statistically significant.

Materials

Unless otherwise noted, all chemicals and reagents were purchased from Sigma-Aldrich (St. Louis, MO, USA). The specific Ano1 inhibitor, T16A$_{inh}$-A01, was purchased from EMD Millipore Biosciences (Billerica, MA, USA).

Results

## A Ca^{2+}- and voltage-dependent macroscopic current was detected in CVECs

A group of macroscopic currents was recorded from mouse CVECs in the presence of a variety concentrations of free $[Ca^{2+}]_i$ (Fig. 1A–F). The current recorded, in the presence of 18 nM free $[Ca^{2+}]_i$, exhibited no outward rectification and time-dependent relaxation (Fig. 1A and G). The amplitude of the outward currents was amplified gradually and the outward rectification and time-dependent relaxation became more profound, as free $[Ca^{2+}]_i$ was increased from 290 nM to 1.1 μM (Fig. 1B–E and G). However, when free $[Ca^{2+}]_i$ reached 36.5 μM, the inward and outward currents were nearly equal in amplitude, and time-dependent relaxation was almost lost (Fig. 1F and G). The macroscopic currents were deactivated by switching membrane potential to –100 mV. The average instantaneous tail current density measured at –100 mV after pre-pulses to different membrane voltage was plotted as a function of free $[Ca^{2+}]_i$ and the data points were fitted to the Hill equation (Fig. 1H). The data show that EC_{50} of free $[Ca^{2+}]_i$ decreased by about fourfold [2.08 ± 1.04 μM at 0 mV (n = 7–11) vs. 0.53 ± 0.06 μM at +100 mV (n = 7–11)]. These results suggest that the gating of the macroscopic currents recorded from CVECs is Ca^{2+}- and voltage-dependent.

A chloride channel mediates the voltage- and Ca^{2+}-dependent currents in CVECs

For the rest of the experiments, 777 nM free $[Ca^{2+}]_i$ was used. We assessed anion selectivity experiments to determine whether the voltage- and Ca^{2+}-dependent macroscopic current is mediated by a chloride channel. The magnitude of outward currents was significantly reduced by replacing extracellular Cl^- with gluconate$^-$, and the V_{rev} shifted from near zero (–1.37 ± 0.79 mV) to depolarizing potential (52.5 ± 2.31 mV) (n = 5) (Fig. 2A–C). Substitution of extracellular Cl^- with NO_3^- resulted in a dramatic increase in the amplitude of outward current, and the V_{rev} shifted from near zero (–0.92 ± 0.68 mV) to hyperpolarizing potentials (–23.11 ± 1.04 mV) (n = 8) (Fig. 2D–F). The relative permeability ratios for P_{glu}/P_{Cl} and P_{NO3}/P_{Cl} were 0.13 ± 0.01 and 2.30 ± 0.10. Moreover, the macroscopic current was reversibly blocked by 100 μM niflumic acid (NFA), a non-specific chloride channel blocker (n = 6) (Fig. 2G–J). These data together suggest that the voltage- and Ca^{2+}-dependent current recorded from CVECs is mediated by a chloride channel.

Ano1 presents in CVECs isolated from neonatal mouse

The biophysical features and pharmacological profile of the $I_{Cl(Ca)}$ detected in CVECs are similar to those of CaCCs. We reasoned that $I_{Cl(Ca)}$ might be mediated by Ano1. As seen in Fig. 3A, Ano1 mRNA, but not Ano2 mRNA, was detected in CVECs (Fig. 3A). Western blot analysis demonstrated that CVECs expressed Ano1 (Fig. 3B). We further stained the neonatal mouse heart with anti-Ano1 antibody and anti-vWF antibody, a marker for endothelial cells, and sliced the left ventricular walls in longitudinal sections. Ano1 (green) was nicely present at endothelium and co-localized with endothe-
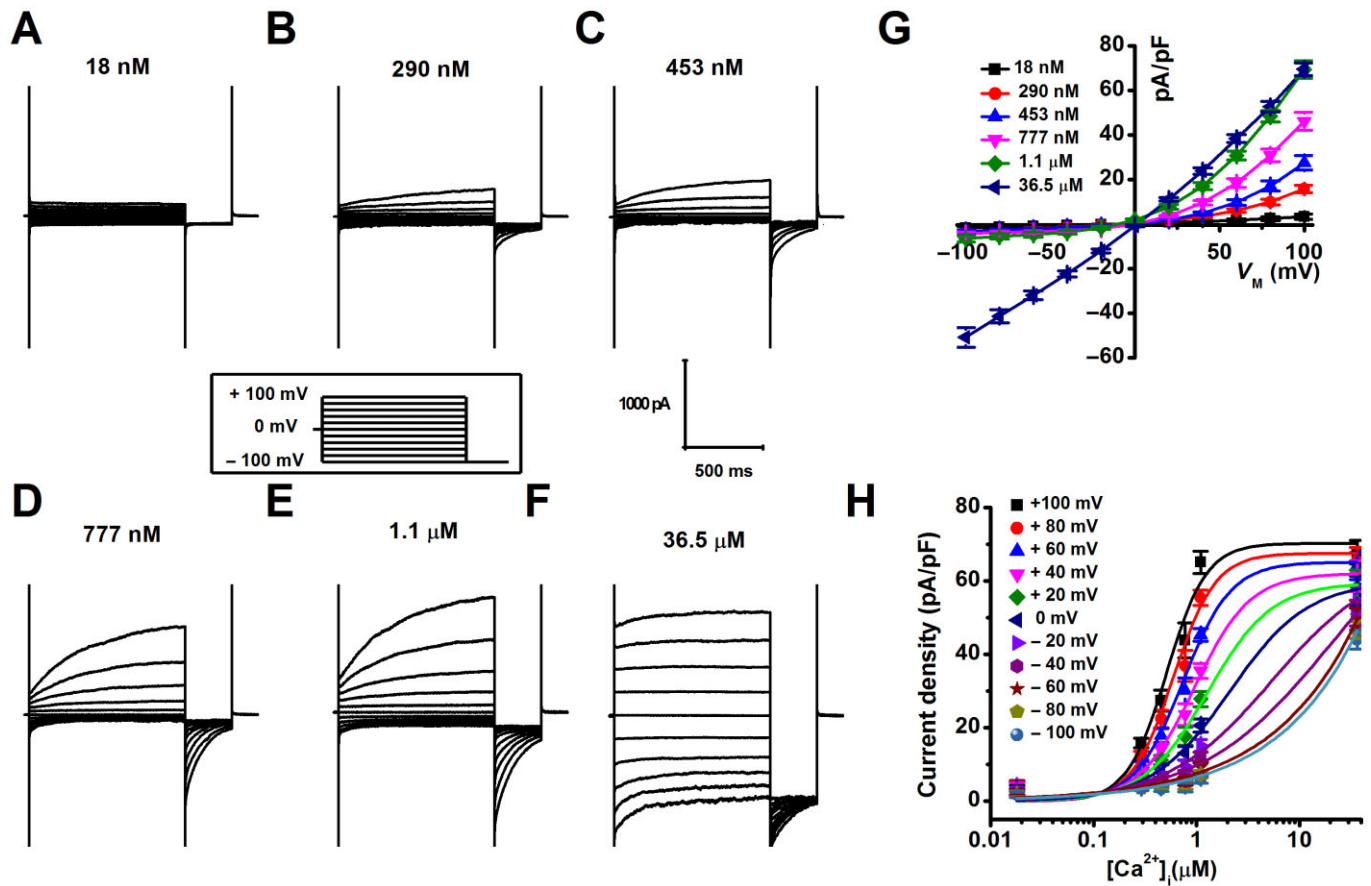
Figure 1

(A–F) Representative macroscopic currents were recorded in CVECs, in the presence of desired free $[Ca^{2+}]_i$, with the voltage protocol shown in the inset. (G) Calculated steady-state current densities, in the presence of a variety of free $[Ca^{2+}]_i$, were plotted as a function of membrane potentials ($n = 5–11$ for different data points). (H) Current densities calculated from tail currents measured at -100 mV after pre-pulses between $+100$ and -100 mV were plotted against $[Ca^{2+}]_i$ and were fitted with the Hill equation ($n = 7–11$ for different data points).

lial marker (red) (Fig. 3C; the white arrow heads indicate blood vessels). Confocal imaging analyses also revealed that a co-localization of Ano1 (green) and CD31 (red) occurred at the plasma membrane of CVECs (Fig. 3D) because the highest merged fluorescence intensity (peaks) appeared in the vicinity of the plasma membrane (Fig. 3E). These results led us to hypothesize that the $I_{Cl(Ca)}$ is carried by Ano1 in CVECs.

The $I_{Cl(Ca)}$ in CVECs is mediated by Ano1

T16A$_{inh}$-A01, a newly identified specific Ano1 inhibitor (Forrest *et al.*, 2012; Davis *et al.*, 2013), and a specific pore-targeting anti-Ano1 antibody (Thomas-Gatewood *et al.*, 2011) were respectively applied to the bath solution to test the hypothesis that the $I_{Cl(Ca)}$ recorded from CVECs is mediated by Ano1. Figure 4A–D showed that the $I_{Cl(Ca)}$ was significantly and reversibly inhibited by 30 μM T16A$_{inh}$-A01 (~60%). The specific pore-targeting Ano1 antibody also dramatically inhibited $I_{Ca(Cl)}$ (~57%) (Fig. 4E–G); however, the boiled-specific pore-targeting, anti-ANO1 antibody had no effect on the amplitude of the $I_{Ca(Cl)}$ (Fig. 4H–J). Furthermore, the $I_{Ca(Cl)}$ was almost completely blocked in Ano1-specific shRNA transfected CVECs; in contrast, the $I_{Ca(Cl)}$ was not altered in CVECs

expressing scramble shRNA (Fig. 4K–N) (refer to Supporting Information Fig. S1 for gene silencing efficiency; since shRNAs were linked with GFP, the cells showing green were used for patch-clamp analyses). These data strongly suggest that the $I_{Ca(Cl)}$ recorded from CVECs is mediated by Ano1.

Hypoxia potentiates Ano1-mediated $I_{Cl(Ca)}$ in CVECs

As shown in Fig. 5A, B, F and G, the steady-state current (I_{ss}) and the instantaneous current (I_{inst}) were significantly potentiated by hypoxia, although with different extent (approximately twofold for I_{ss} and approximately fourfold for I_{inst} at depolarizing potentials). Hypoxia-induced increased in the amplitude of $I_{Ca(Cl)}$ was significantly inhibited by the specific pore-targeting Ano1 antibody (Fig. 5C, F and G) and by T16A$_{inh}$-A01 (data not shown). Moreover, hypoxia also significantly enhanced the amplitude of $I_{Ca(Cl)}$ in Ano1 knockdown CVECs (Fig. 5D and E; *I–V* data not shown), suggesting that the residual Ano1 was up-regulated by hypoxia. These data further confirm that the $I_{Ca(Cl)}$ recorded in CVECs is mediated by Ano1. The data shown in Fig. 5H and I demonstrate that the mRNA and protein expression levels of Ano1
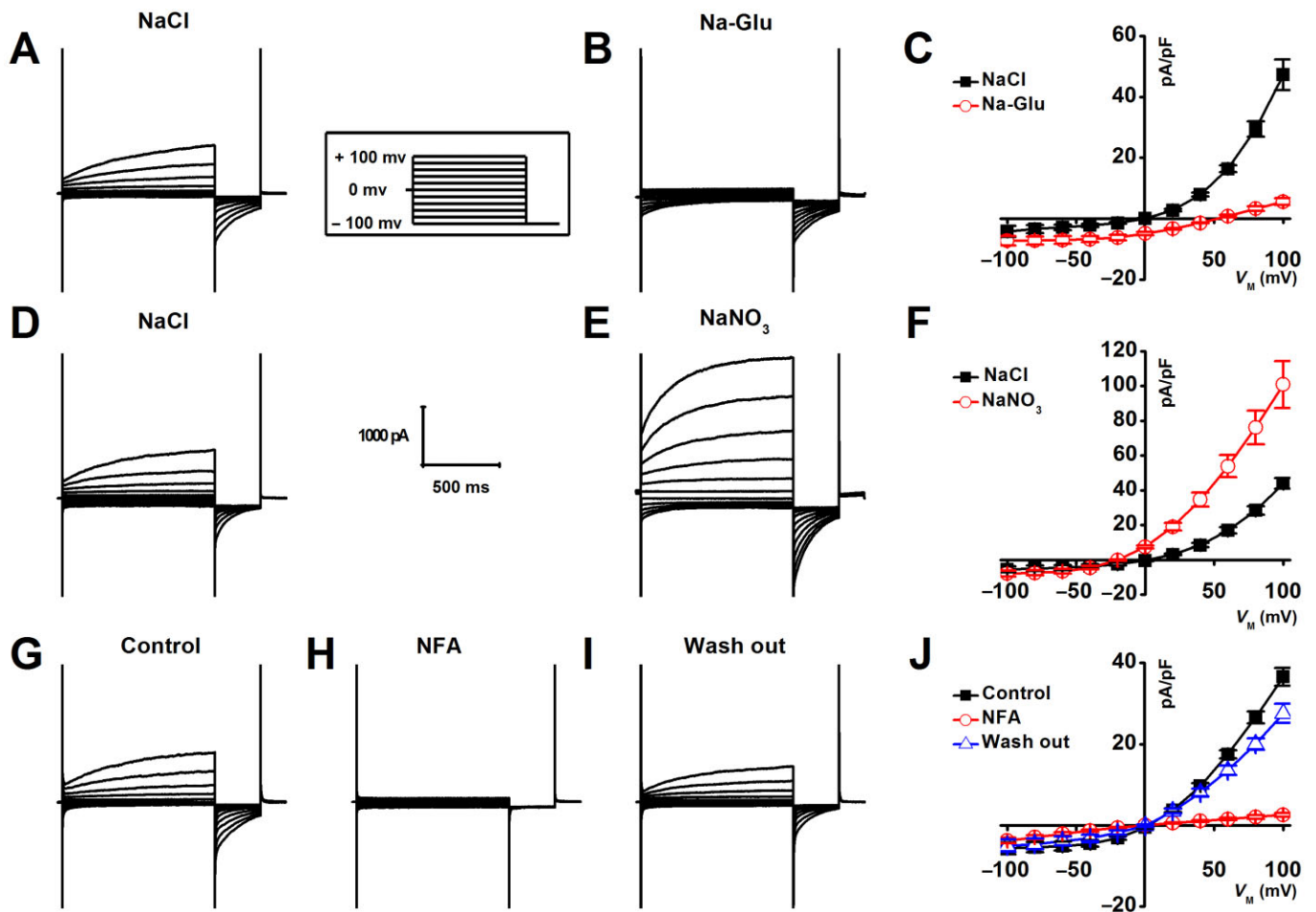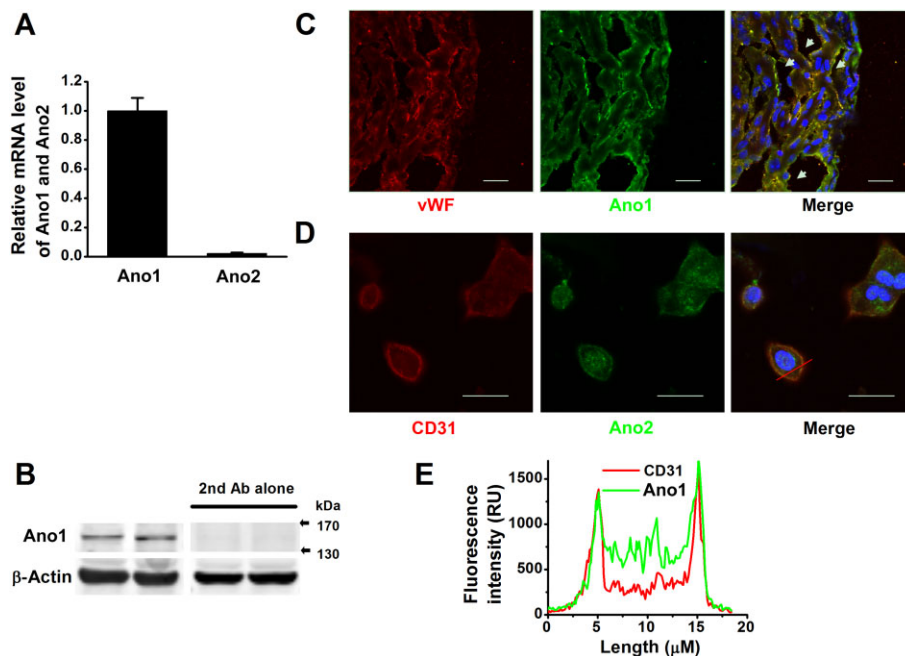
Figure 2

Representative macroscopic current traces were respectively recorded from CVECs with the voltage protocol depicted in the inset, in the presence of NaCl (A and D), Na-gluconate (B) or NaNO₃ (E). The steady-state current densities obtained from indicated experimental conditions were plotted as a function of membrane potentials (C and F) ($n = 5$–8 for different data points). (G–I) Representative macroscopic current traces were respectively recorded from a CVEC under control condition (G) or in the presence of 100 μM NFA (H), and followed by washing out NFA (I). (J) Steady-state *I*–*V* relationships show that the current was significantly blocked by 100 μM NFA ($n = 6$).

were slightly, but significantly increased by exposure of CVECs to hypoxia. However, the increased Ano1 protein expression levels (~20%) were not in agreement with hypoxia-induced increase in current density (approximately twofold for I_{ss} and approximately fourfold for I_{inst}), suggesting that there might be other mechanisms by which hypoxia induces an increase in the current density of Ano1. Moreover, the proliferation rate of CVECs was increased ~20% by hypoxia. This hypoxia-induced increase in proliferation rate was not affected by T16A$_{inh}$-A01 in either control cells or in the cells exposed to hypoxia (Fig. 5J).

Hypoxia amplifies the current density of Ano1 via enhancing its sensitivity to Ca²⁺ and to membrane voltage

Figure 6A shows that in hypoxic CVECs, the ratios of I_{inst}/I_{ss} (obtained from the records shown in Fig. 5A and B) were increased by hypoxia at the depolarizing potentials. Furthermore, the average τ_{act} values were significantly smaller in the

cells exposed to hypoxia than in control cells (Fig. 6B). These data suggest that hypoxia alters the activation kinetics of Ano1 in CVECs during sustained depolarization, which is sensitive to Ca²⁺ (Kuruma and Hartzell, 2000; Xiao *et al.*, 2011). The τ_{inact} values were increased in CVECs exposed to the hypoxia, suggesting that hypoxia retarded the deactivation of Ano1 channels (Fig. 6E). Furthermore, EC$_{50}$ of [Ca²⁺]$_i$ for activating Ano1-mediated $I_{Ca(Cl)}$ was 534 ± 63.2 nM for control ($n = 7$–11 for different data points) and 385 ± 35.4 nM for hypoxia ($n = 6$–8 for different data points) ($P < 0.05$), with Hill coefficients of 2.20 for control and 4.33 for hypoxia (Fig. 6F). The data described earlier suggest that hypoxia potentiates the sensitivity of Ano1-mediated $I_{Ca(Cl)}$ to Ca²⁺, for example, activation of Ano1-mediated $I_{Ca(Cl)}$ requires much lower [Ca²⁺]$_i$ under hypoxic condition. Figure 6G shows that the half maximum activation voltage ($V_{1/2}$) was shifted from 103 ± 10 mV for control ($n = 11$) to 8.21 ± 2.30 mV for hypoxia ($n = 8$) ($P < 0.01$), with the corresponding slope factor (k) values of 42.77 ± 2.10 and 53.01 ± 2.61, respectively,

Figure 3

(A) qRT-PCR demonstrates the relative mRNA levels of Ano1 and Ano2 in CVECs ($n = 6$); Ano1, but not Ano2, was expressed in CVECs. (B) Western blots shown at the two left panels indicate CVECs express Ano1; with the secondary antibody alone, no band was detected (two panels at right) (repeated five times). (C) Representative immunofluorescence images of the sliced left ventricular wall in longitudinal section, labelled with antibodies raised against vWF (red) and against Ano1 (green). The white arrow heads indicate blood vessels. (D) Representative immunofluorescence images of isolated CVECs labelled with antibodies raised against CD31 (red) and against Ano1 (green). Scale bar represents 20 μm. (E) The representative fluorescence intensity histograms, constructed across a CVEC [the red solid line shown in (D)]. The majority of Ano1 (green) was distributed at and/or in the vicinity of the plasma membrane.

suggesting that hypoxia enhances sensitivity of Ano1-mediated $I_{Ca(Cl)}$ to membrane voltage, for example, activation of Ano1-mediated $I_{Ca(Cl)}$ requires significantly less membrane depolarization.

Hypoxia induces an altered expression ratio of the Ano1 variants

The human Ano1 splicing variants (deletion of exons 6b, 13 and 15) are known to generate the currents with distinct biophysical properties to wild-type Ano1 (Ferrera *et al.*, 2009; Mazzone *et al.*, 2011). Furthermore, there are a variety of Ano1 splicing variants in mouse heart and these splicing events are highly conserved between human and mouse (O'Driscoll *et al.*, 2011). Therefore, we examined whether hypoxia may cause the changes in the ratio of Ano1 splicing variants, which, in turn, alter the biophysical properties of Ano1-mediated $I_{Ca(Cl)}$. Our qRT-PCR data showed that under hypoxic condition, the mRNA expression levels of Ano1 splicing variants lacking of exons 6b and 13 (Fig. 7A and B), but not lacking exon 15 (Fig. 7C), were significantly higher than those of control (the primers used are listed in Supporting Information Table S2). These results suggest that changes in the ratio of Ano1 splicing variants may involve in the altered biophysical properties of Ano1-mediated $I_{Ca(Cl)}$ under hypoxic condition.

Discussion

The major findings of the present study are as follows: (i) demonstrating that mouse CVECs express Ano1; (ii) the $I_{Cl(Ca)}$ recorded from CVECs is mediated by Ano1 and the biophysical properties of the Ano1-encoded $I_{Cl(Ca)}$ are compatible with those of CaCCs; (iii) hypoxia up-regulates Ano1-mediated $I_{Cl(Ca)}$ via enhancing its expression levels and an altered expression ratio of Ano1 splicing variants, thereby potentiating its sensitivity to Ca^{2+} and the membrane voltage.

Although the $I_{Cl(Ca)}$ in endothelial cells was discovered more than 20 years ago, its molecular identity remains uncertain (Hartzell *et al.*, 2005). Therefore, we aimed to identify the gene responsible for CaCCs in mouse CVECs. We detected a NFA-sensitive macroscopic current with profound outward rectification, time-dependent relaxation and an anionic selectivity sequence of $NO_3^- > Cl^- > Glu^-$. The gating of this macroscopic current was dependent upon Ca^{2+} and upon membrane voltage. These data suggest that the macroscopic current detected in CVECs is an $I_{Cl(Ca)}$. The biophysical features of the $I_{Cl(Ca)}$ in CVECs are consistent with what has been reported for CaCC (Qu *et al.*, 2003). The results obtained from qRT-PCR, Western blot and immunofluorescence imaging analyses suggest that Ano1 is present in CVECs. The $I_{Cl(Ca)}$ recorded from CVECs was reversibly blocked by T16A$_{inh}$-A01, a specific Ano1 inhibitor (Forrest *et al.*, 2012; Davis *et al.*,
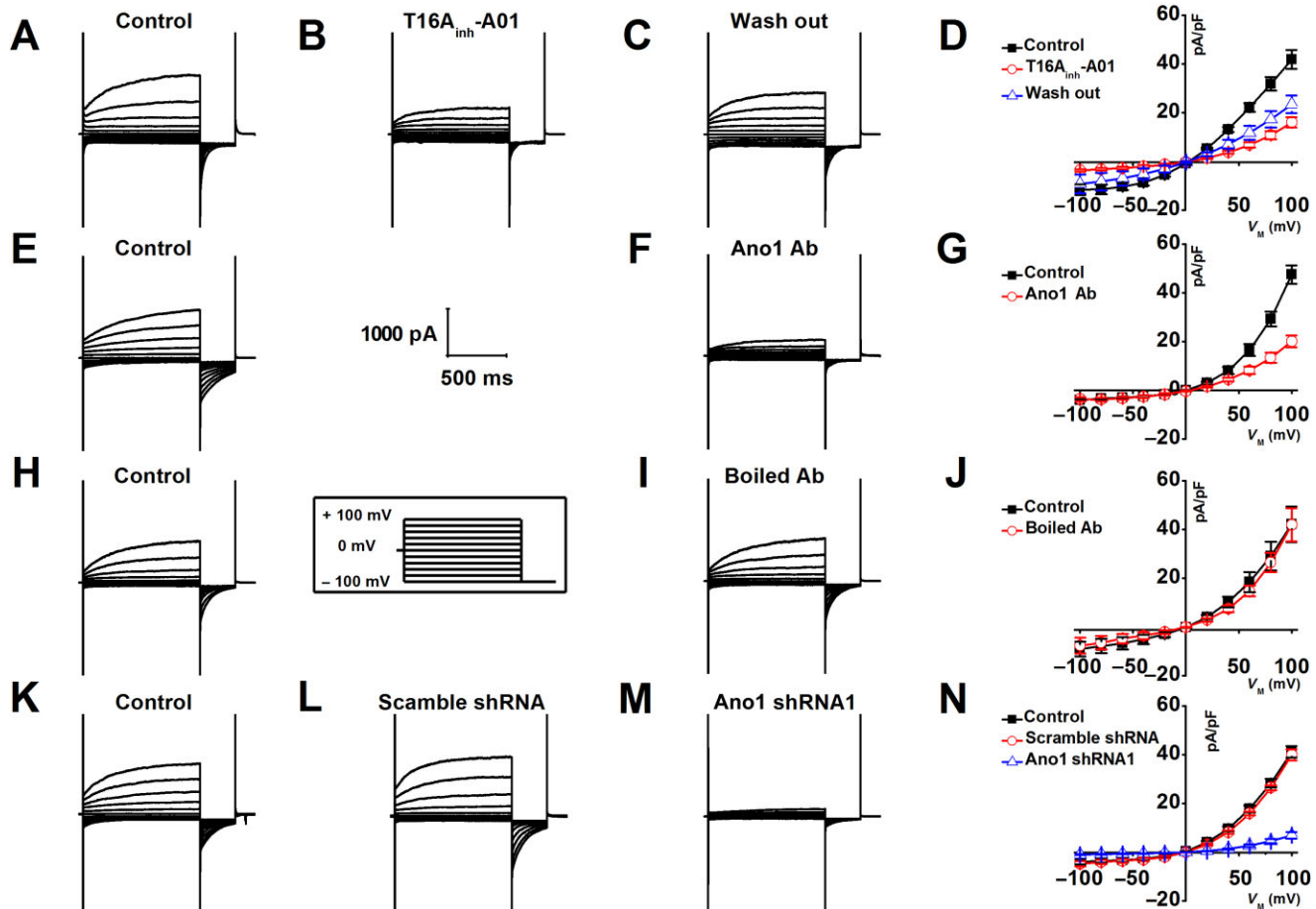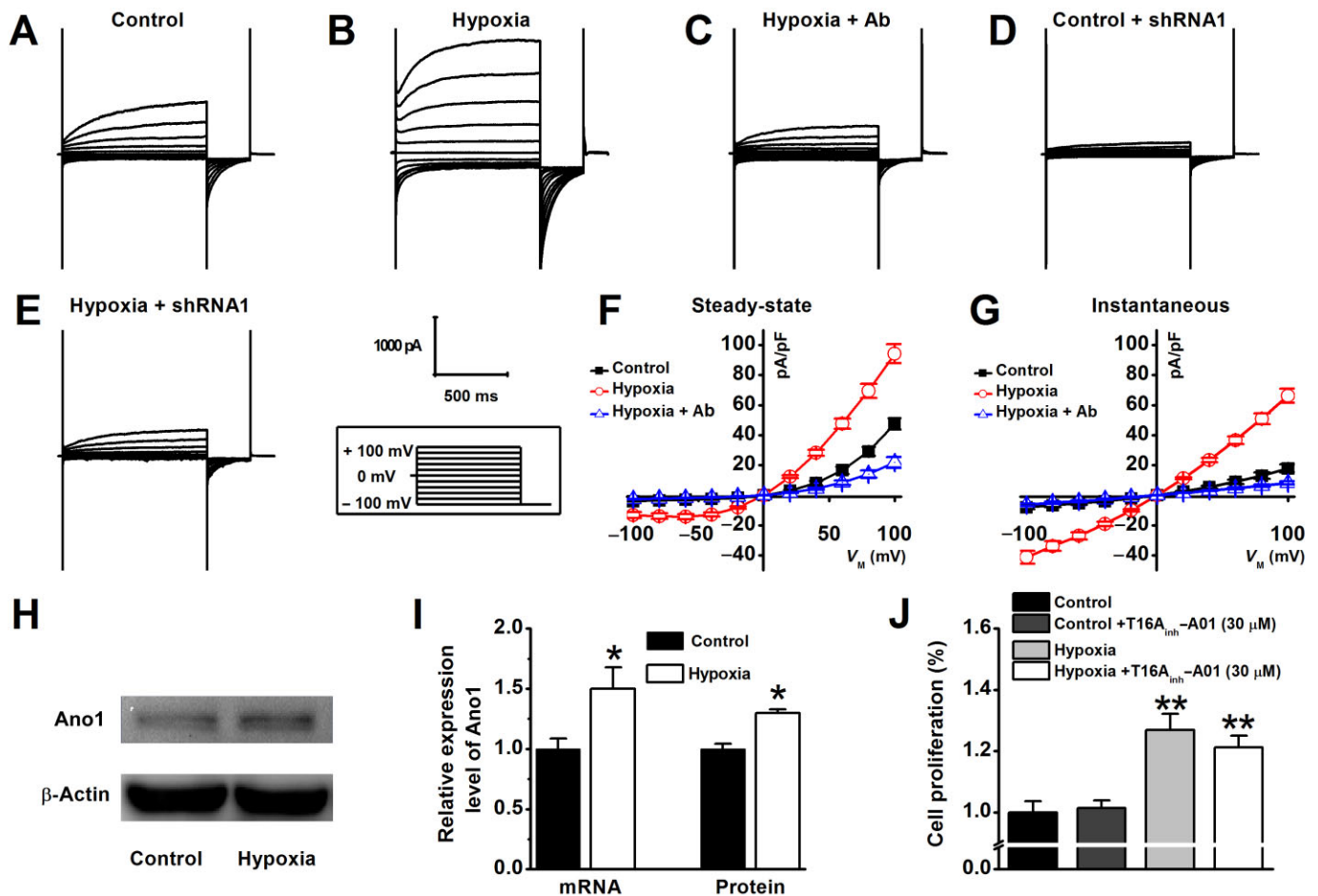
Figure 4

(A–C) Representative macroscopic currents were respectively generated in the same cell under control condition, in the presence of 30 μM T16A$_{inh}$-A01 followed by washing out. (D) Steady-state current densities obtained from indicated experimental conditions were plotted as a function of the membrane voltages. The macroscopic currents were significantly and reversibly inhibited by T16A$_{inh}$-A01 ($n = 5$). (E and F) Representative whole-cell currents were recorded from the same cell under control condition and 10 min after application of specific pore-targeting anti-Ano1 antibody. (G) I–V relationships show that the macroscopic currents were significantly inhibited by anti-Ano1 antibody ($n = 6$). (H and I) Representative macroscopic currents were respectively obtained from the same cell, in the absence or in the presence of boiled anti-Ano1 antibody. (J) I–V relationships show that the boiled anti-Ano1 antibody did not affect the macroscopic current density ($n = 6$). (K–M) Representative macroscopic currents were respectively generated from control cells ($n = 8$), the cells transfected with scramble shRNA ($n = 6$) and the cells transfected with shRNA against Ano1 ($n = 6$). (N) I–V relationships show that the macroscopic currents were greatly diminished in Ano1 knockdown CVECs.

2013), and was significantly inhibited by a specific pore-targeting anti-Ano1 antibody (Thomas-Gatewood *et al.*, 2011) and was greatly diminished in Ano1 knockdown CVECs. Furthermore, hypoxia-induced augmentation of the $I_{Cl(Ca)}$ was completely inhibited by the specific pore-targeting anti-Ano1 antibody. These results strongly suggest that the $I_{Cl(Ca)}$ recorded from mouse CVECs is mediated by Ano1.

Recent reports suggest that translation of mouse Ano1 yields a molecular weight of ~110 kDa (Davis *et al.*, 2010). The exclusion of exon 18 in the mouse transcript could result in a truncated Ano1 protein of ~60–75 kDa (O'Driscoll *et al.*, 2011). We have to notice that the molecular weight of Ano1 in mouse CVECs, detected by Western blots, is ~150 kDa, which is similar to those described in distal colonic epithelial cells and neck squamous cell carcinoma (He *et al.*, 2011; Duvvuri *et al.*, 2012). Human Ano1 has various protein iso-

forms generated by alternative splicing and has been labelled the four identified alternative segments as a, b, c and d (Ferrera *et al.*, 2009). The TMEM16 (abc)-mediated channel was strongly inactivated by 1.25 μM Ca^{2+} (Ferrera *et al.*, 2011). In comparison, we were able to generate Ano1 current at 36.5 μM Ca^{2+}, albeit with no outward rectification and time-dependent relaxation. Our result is very compatible with those obtained from HEK293 cells overexpressing Ano1 (Xiao *et al.*, 2011). Our data show that mouse Ano1 has a much lower EC$_{50}$ for Ca^{2+} (~0.53 μM at +100 mV) compared with those human varieties of Ano1 [~3.32 μM for (abc) and ~0.85 μM for (ac)] (Ferrera *et al.*, 2009). It is no surprise because alternative splicing events are thought to affect Ca^{2+} sensitivity, voltage dependence and the kinetics of activation and deactivation of the Ano1 channel (Ferrera *et al.*, 2009; 2011; Xiao *et al.*, 2011).
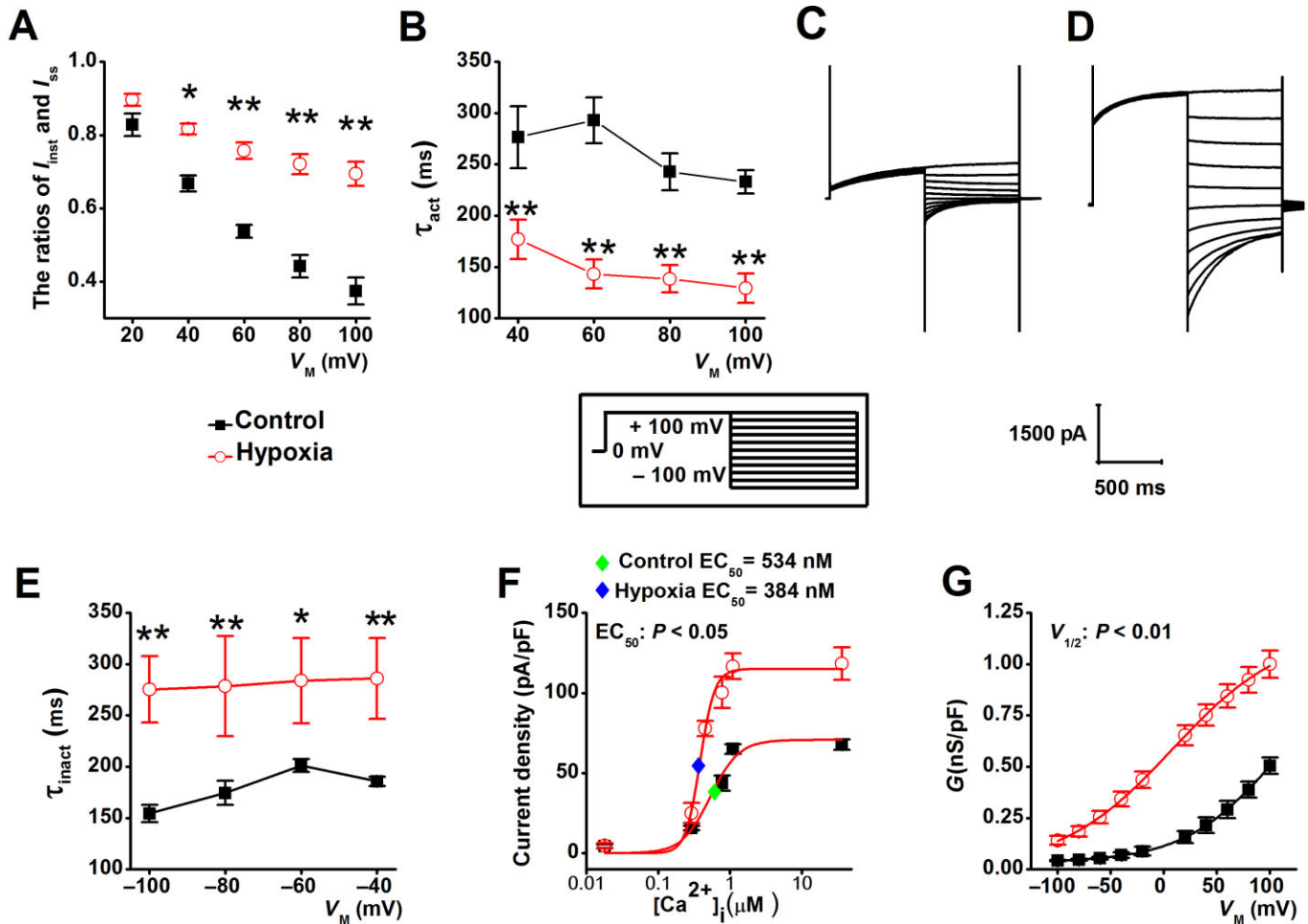
Figure 5

Representative macroscopic currents were respectively recorded from control cells (A), cells exposed to hypoxia in the absence (B) or in the presence of anti-Ano1 antibody ($n = 6$) (C), from Ano1 knockdown cells ($n = 6$) (D), the cells exposed to hypoxia ($n = 7$) (E). (F and G) The densities of I_{ss} and I_{inst} were plotted versus membrane potentials; the data show that the densities of I_{ss} and I_{inst} were potentiated by approximately twofold and fourfold, respectively, by hypoxia and were dramatically inhibited by anti-Ano1 antibody. (H) Western blots demonstrating the expression levels of Ano1 under control and hypoxic condition. (I) Summarized bar graph demonstrates that the expression levels of Ano1 mRNA and protein were up-regulated by hypoxia ($n = 7$). (J) MTT assays demonstrating the cell proliferation rate under different experimental conditions ($n = 6$ for each set of experiment). *$P < 0.05$, **$P < 0.01$, significantly different from control.

Hypoxia is associated with angina pectoris, myocardial infarction, heart failure and peripheral artery disease. Severe hypoxia induces cell proliferation and angiogenesis (Li *et al.*, 2007). Vascular endothelial cell proliferation plays an essential role in angiogenesis and revascularization of the myocardium following myocardial infarction (Isner and Losordo, 1999). Sun and co-workers suggested that an increase in expression levels of Ano1 in SMCs, isolated from chronic-hypoxic pulmonary hypertension rat, is responsible for enhanced current density of Ano1 (Sun *et al.*, 2012). A similar result was observed in monocrotaline-induced pulmonary hypertension rat model (Forrest *et al.*, 2012). In comparison, our results demonstrate that hypoxia enhances the density of Ano1-mediated $I_{Cl(Ca)}$ not only through increasing expression of Ano1 but also through potentiating its sensitivity to Ca^{2+} and to membrane voltage. Recent studies suggest that a variety of Ano1 splicing variants are present in mouse heart (O'Driscoll *et al.*, 2011). Therefore, we speculated that the

hypoxia-induced increase in Ano1 expression levels and altered biophysical features of Ano1 in CVECs might be associated with the changes in the ratio of Ano1 splicing variants. We found that the relative mRNA expression levels of exons 6b and 13 excluded Ano1 variants were significantly up-regulated by hypoxia. Due to overexpression of exon 6b, omitted human Ano1 in HEK293 cells led to a significantly increased sensitivity to Ca^{2+} (Ferrera *et al.*, 2009); we also speculate that hypoxia-induced increase in Ca^{2+} sensitivity of Ano1-mediated $I_{Cl(Ca)}$ could be attributable to elevated expression levels of exon 6b excluded Ano1 variant in CVECs. Furthermore, hypoxia-induced increase in voltage sensitivity of Ano1-mediated $I_{Cl(Ca)}$ might be caused by the increased fraction of exon 13 excluded Ano1 variant, since a reduction of the voltage dependence of activation was found in HEK293 cells expressing exon 13 deleted human Ano1 variant (Ferrera *et al.*, 2009). Overexpression of exon 15 deleted human Ano1 variant in HEK293 resulted in a significant faster activation
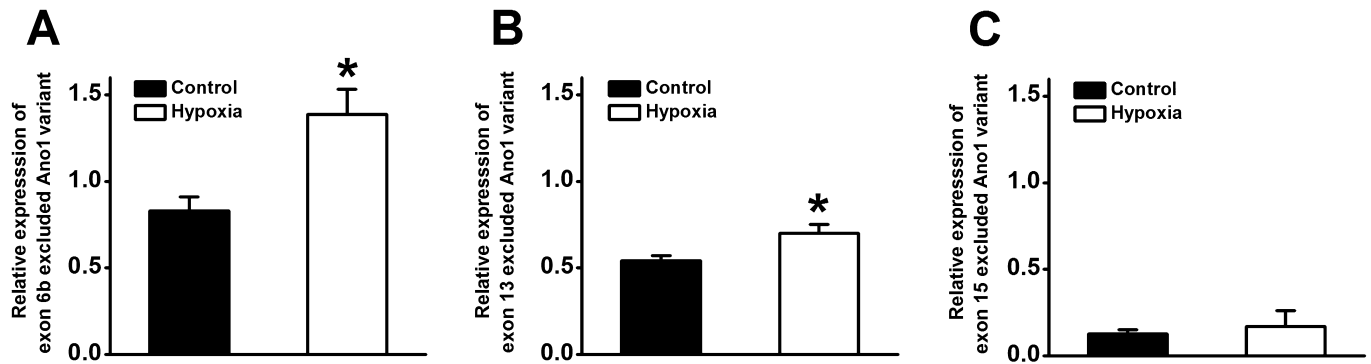
Figure 6

(A) The ratios of I_{inst} and I_{ss} obtained from control ($n = 11$) and cells exposed to hypoxia ($n = 11$) were plotted against voltage. (B) Average τ_{act} obtained from control (as shown in Fig. 5A; $n = 11$) and hypoxic cells (as shown in Fig. 5B; $n = 11$) was plotted against voltage. (C and D) Representative macroscopic currents were respectively recorded from the CVECs under the control and hypoxic conditions using a voltage protocol shown in inset. (E) Average τ_{inact} obtained from control (shown in C; $n = 6$) and hypoxic (shown in D; $n = 5$) cells was plotted versus voltage. (F) Current densities calculated from tail currents measured at -100 mV after pre-pulses between $+100$ and -100 mV in control and hypoxic cells (from the records as shown in Fig. 5A and 5B) were plotted against $[Ca^{2+}]_i$ and were respectively fitted with the Hill equation. The blue and green diamonds, respectively, indicate the mean EC_{50} of $[Ca^{2+}]_i$ for activating Ano1-mediated $I_{Ca(Cl)}$ in control ($n = 7$–11) and hypoxia CVECs ($n = 6$–8). (G) The G was plotted against each tested potential and the data points were fitted to the Boltzmann function to obtain mean steady-state activation curves ($n = 11$ for control; $n = 8$ for hypoxia).

and deactivation kinetics (Mazzone *et al.*, 2011). However, we did not detect if hypoxia caused changes in the relative ratio of exon 15 excluded Ano1 variant in CVECs. Finally, this hypoxia-induced increase in Ano1 current density might be, at least in part, due to Ca^{2+} overload under this condition (Abdallah *et al.*, 2007).

Ano1 may be involved in hypertension-induced cerebrovascular remodelling, based upon the facts that knockdown of Ano1 facilitates and overexpression of Ano1 inhibits angiotensin II-induced cell cycle transition and cell proliferation in rat basilar SMCs (Wang *et al.*, 2012). Other studies suggest that the function of Ano1 is an important factor for contraction of SMCs both in membrane potential-dependent and membrane potential-independent ways (Dam *et al.*, 2013). Several studies have suggested that Ano1 expression

levels are associated with cell proliferation including interstitial cells of Cajal in the small intestine (Stanich *et al.*, 2011), head and neck squamous cell carcinoma cells, the T24 bladder cancer cells (Duvvuri *et al.*, 2012) and the gastrointestinal stromal tumour cells (Simon *et al.*, 2013). Our data suggest that hypoxia also induces an increase in the proliferation rate of CVECs; however, it appears that this hypoxia-induced proliferation is not due to enhanced Ano1 activity because T16A$_{inh}$-A01 (up to 30 μM for 48 h) did not affect the cell growth.

In summary, we suggest that Ano1 forms CaCC in CVECs and that hypoxia up-regulates Ano1-mediated $I_{Cl(Ca)}$ via enhancing its expression levels and an altered expression ratio of Ano1 splicing variants, thereby potentiating its sensitivity to Ca^{2+} and the membrane voltage.

Figure 7

qRT-PCR demonstrating hypoxia induces an altered expression ratio of Ano1 splicing variants in CVECs. (A and B) The relative mRNA expression levels of exons 6b and 13 excluded Ano1 were significantly up-regulated by hypoxia ($n = 7$). (C) Hypoxia did not affect the expression levels of exon 15 excluded Ano1 ($n = 7$). *$P < 0.05$, significantly different from control.

Author contributions

Z-RZ, DZ and DDD conceived and designed the experiments; M-MW, JL, B-LS, Y-FG, Y-CL, CY, Q-SW, T-XM and KM collected, analysed and interpreted the data; Z-RZ, DZ and M-MW drafted the manuscript; HCH and DDD revised the manuscript; and all authors approved the final version of the manuscript.

Conflict of interest

None declared.

References

Abdallah Y, Gligorievski D, Kasseckert SA, Dieterich L, Schafer M, Kuhlmann CR et al. (2007). The role of poly(ADP-ribose) polymerase (PARP) in the autonomous proliferative response of endothelial cells to hypoxia. Cardiovasc Res 73: 568–574.

Alexander SPH, Benson HE, Faccenda E, Pawson AJ, Sharman JL, Catterall WA et al. (2013). The Concise Guide to PHARMACOLOGY 2013/14: Ion Channels. Br J Pharmacol 170: 1607–1651.

Caputo A, Caci E, Ferrera L, Pedemonte N, Barsanti C, Sondo E et al. (2008). TMEM16A, a membrane protein associated with calcium-dependent chloride channel activity. Science 322: 590–594.

Dam VS, Boedtkjer DM, Nyvad J, Aalkjaer C, Matchkov V (2013). TMEM16A knockdown abrogates two different Ca-activated Cl currents and contractility of smooth muscle in rat mesenteric small arteries. Pflugers Arch doi:10.1007/s00424-013-1382-1.

Davis AJ, Forrest AS, Jepps TA, Valencik ML, Wiwchar M, Singer CA et al. (2010). Expression profile and protein translation of TMEM16A in murine smooth muscle. Am J Physiol Cell Physiol 299: C948–C959.

Davis AJ, Shi J, Pritchard HA, Chadha PS, Leblanc N, Vasilikostas G et al. (2013). Potent vasorelaxant activity of the TMEM16A inhibitor T16A(inh) -A01. Br J Pharmacol 168: 773–784.

Dutta AK, Khimji AK, Kresge C, Bugde A, Dougherty M, Esser V et al. (2011). Identification and functional characterization of TMEM16A, a Ca²⁺-activated Cl⁻ channel activated by extracellular nucleotides, in biliary epithelium. J Biol Chem 286: 766–776.

Duvvuri U, Shiwarski DJ, Xiao D, Bertrand C, Huang X, Edinger RS et al. (2012). TMEM16A induces MAPK and contributes directly to tumorigenesis and cancer progression. Cancer Res 72: 3270–3281.

Ferrera L, Caputo A, Ubby I, Bussani E, Zegarra-Moran O, Ravazzolo R et al. (2009). Regulation of TMEM16A chloride channel properties by alternative splicing. J Biol Chem 284: 33360–33368.

Ferrera L, Scudieri P, Sondo E, Caputo A, Caci E, Zegarra-Moran O et al. (2011). A minimal isoform of the TMEM16A protein associated with chloride channel activity. Biochim Biophys Acta 1808: 2214–2223.

Forrest AS, Joyce TC, Huebner ML, Ayon RJ, Wiwchar M, Joyce J et al. (2012). Increased TMEM16A-encoded calcium-activated chloride channel activity is associated with pulmonary hypertension. Am J Physiol Cell Physiol 303: C1229–C1243.

Hartzell C, Putzier I, Arreola J (2005). Calcium-activated chloride channels. Annu Rev Physiol 67: 719–758.

Hartzell HC, Yu K, Xiao Q, Chien LT, Qu Z (2009). Anoctamin/TMEM16 family members are Ca²⁺-activated Cl⁻ channels. J Physiol 587 (Pt 10): 2127–2139.

He Q, Halm ST, Zhang J, Halm DR (2011). Activation of the basolateral membrane Cl^- conductance essential for electrogenic K^+ secretion suppresses electrogenic Cl^- secretion. Exp Physiol 96: 305–316.

Hille B (1992) Ionic Channels of Excitable Membranes, 2nd edn. Sinauer Associates: Sunderland, MA.

Hosoki E, Iijima T (1994). Chloride-sensitive Ca^{2+} entry by histamine and ATP in human aortic endothelial cells. Eur J Pharmacol 266: 213–218.

Huang F, Rock JR, Harfe BD, Cheng T, Huang X, Jan YN *et al.* (2009). Studies on expression and function of the TMEM16A calcium-activated chloride channel. Proc Natl Acad Sci U S A 106: 21413–21418.

Hwang SJ, Blair PJ, Britton FC, O'Driscoll KE, Hennig G, Bayguinov YR *et al.* (2009). Expression of anoctamin 1/TMEM16A by interstitial cells of Cajal is fundamental for slow wave activity in gastrointestinal muscles. J Physiol 587 (Pt 20): 4887–4904.

Isner JM, Losordo DW (1999). Therapeutic angiogenesis for heart failure. Nat Med 5: 491–492.

Kilkenny C, Browne W, Cuthill IC, Emerson M, Altman DG (2010). Animal research: reporting *in vivo* experiments: the ARRIVE guidelines. Br J Pharmacol 160: 1577–1579.

Kuruma A, Hartzell HC (2000). Bimodal control of a $Ca(2+)$-activated $Cl(-)$ channel by different $Ca(2+)$ signals. J Gen Physiol 115: 59–80.

Li W, Petrimpol M, Molle KD, Hall MN, Battegay EJ, Humar R (2007). Hypoxia-induced endothelial proliferation requires both mTORC1 and mTORC2. Circ Res 100: 79–87.

McGrath JC, Drummond GB, McLachlan EM, Kilkenny C, Wainwright CL (2010). Guidelines for reporting experiments involving animals: the ARRIVE guidelines. Br J Pharmacol 160: 1573–1576.

Manoury B, Tamuleviciute A, Tammaro P (2010). TMEM16A/anoctamin 1 protein mediates calcium-activated chloride currents in pulmonary arterial smooth muscle cells. J Physiol 588 (Pt 13): 2305–2314.

Mazzone A, Bernard CE, Strege PR, Beyder A, Galietta LJ, Pasricha PJ *et al.* (2011). Altered expression of Ano1 variants in human diabetic gastroparesis. J Biol Chem 286: 13393–13403.

Nilius B, Prenen J, Szucs G, Wei L, Tanzi F, Voets T *et al.* (1997). Calcium-activated chloride channels in bovine pulmonary artery endothelial cells. J Physiol 498 (Pt 2): 381–396.

O'Driscoll KE, Pipe RA, Britton FC (2011). Increased complexity of Tmem16a/Anoctamin 1 transcript alternative splicing. BMC Mol Biol 12: 35.

Ono K, Nakao M, Iijima T (1998). Chloride-sensitive nature of the histamine-induced Ca^{2+} entry in cultured human aortic endothelial cells. J Physiol 511 (Pt 3): 837–849.

Ousingsawat J, Martins JR, Schreiber R, Rock JR, Harfe BD, Kunzelmann K (2009). Loss of TMEM16A causes a defect in epithelial Ca^{2+}-dependent chloride transport. J Biol Chem 284: 28698–28703.

Pifferi S, Dibattista M, Menini A (2009). TMEM16B induces chloride currents activated by calcium in mammalian cells. Pflugers Arch 458: 1023–1038.

Qu Z, Wei RW, Hartzell HC (2003). Characterization of Ca^{2+}-activated Cl^- currents in mouse kidney inner medullary collecting duct cells. Am J Physiol Renal Physiol 285: F326–F335.

Rock JR, O'Neal WK, Gabriel SE, Randell SH, Harfe BD, Boucher RC *et al.* (2009). Transmembrane protein 16A (TMEM16A) is a Ca^{2+}-regulated Cl^- secretory channel in mouse airways. J Biol Chem 284: 14875–14880.

Romanenko VG, Catalan MA, Brown DA, Putzier I, Hartzell HC, Marmorstein AD *et al.* (2010). Tmem16A encodes the Ca^{2+}-activated Cl^- channel in mouse submandibular salivary gland acinar cells. J Biol Chem 285: 12990–13001.

Schroeder BC, Cheng T, Jan YN, Jan LY (2008). Expression cloning of TMEM16A as a calcium-activated chloride channel subunit. Cell 134: 1019–1029.

Simon S, Grabellus F, Ferrera L, Galietta L, Schwindenhammer B, Muhlenberg T *et al.* (2013). DOG1 regulates growth and IGFBP5 in gastrointestinal stromal tumors. Cancer Res 73: 3661–3670.

Stanich JE, Gibbons SJ, Eisenman ST, Bardsley MR, Rock JR, Harfe BD *et al.* (2011). Ano1 as a regulator of proliferation. Am J Physiol Gastrointest Liver Physiol 301: G1044–G1051.

Suh SH, Vennekens R, Manolopoulos VG, Freichel M, Schweig U, Prenen J *et al.* (1999). Characterisation of explanted endothelial cells from mouse aorta: electrophysiology and Ca^{2+} signalling. Pflugers Arch 438: 612–620.

Sun H, Xia Y, Paudel O, Yang XR, Sham JS (2012). Chronic hypoxia-induced upregulation of Ca^{2+}-activated Cl^- channel in pulmonary arterial myocytes: a mechanism contributing to enhanced vasoreactivity. J Physiol 590 (Pt 15): 3507–3521.

Thomas-Gatewood C, Neeb ZP, Bulley S, Adebiyi A, Bannister JP, Leo MD *et al.* (2011). TMEM16A channels generate $Ca(2)$-activated Cl currents in cerebral artery smooth muscle cells. Am J Physiol Heart Circ Physiol 301: H1819–H1827.

Wang M, Yang H, Zheng LY, Zhang Z, Tang YB, Wang GL *et al.* (2012). Downregulation of TMEM16A calcium-activated chloride channel contributes to cerebrovascular remodeling during hypertension by promoting basilar smooth muscle cell proliferation. Circulation 125: 697–707.

Xiao Q, Yu K, Perez-Cornejo P, Cui Y, Arreola J, Hartzell HC (2011). Voltage- and calcium-dependent gating of TMEM16A/Ano1 chloride channels are physically coupled by the first intracellular loop. Proc Natl Acad Sci U S A 108: 8891–8896.

Yang YD, Cho H, Koo JY, Tak MH, Cho Y, Shim WS *et al.* (2008). TMEM16A confers receptor-activated calcium-dependent chloride conductance. Nature 455: 1210–1215.

Yu K, Lujan R, Marmorstein A, Gabriel S, Hartzell HC (2010). Bestrophin-2 mediates bicarbonate transport by goblet cells in mouse colon. J Clin Invest 120: 1722–1735.

Zhong N, Fang QZ, Zhang Y, Zhou ZN (2000). Volume- and calcium-activated chloride channels in human umbilical vein endothelial cells. Acta Pharmacol Sin 21: 215–220.

Zhou Y, Zhang Y, Gao F, Guo F, Wang J, Cai W *et al.* (2010). N-n-butyl haloperidol iodide protects cardiac microvascular endothelial cells from hypoxia/reoxygenation injury by down-regulating Egr-1 expression. Cell Physiol Biochem 26: 839–848.

Supporting information

Additional Supporting Information may be found in the online version of this article at the publisher's web-site:

http://dx.doi.org/10.1111/bph.12730

Figure S1 (A) Immunofluorescence images demonstrate the transfection efficiency. Images were taken by fluorescence microscope. The green colour represents GFP. Scale bars represent 40 μm. (B) qRT-PCR demonstrating the expression levels of Ano1 mRNA under indicated conditions ($n = 6$). (C) Representative immunoblots demonstrating the expression levels of Ano1 protein under different experimental conditions. (D) Summarized bar graph represents the abundance of Ano1 protein under different experimental conditions as indicated ($n = 6$). **Indicates $P < 0.01$ compared to either control or scramble shRNA transfected group.

Table S1 Specific shRNAs sequences for Ano1.

Table S2 Primers used for qRT-PCR of Ano1 exon variants.

Table S3 Oligo nucleotide primers for qRT-PCR.

Appendix S1 Methods and results.